Modified Inverted Microstrip Integrated Filter

Nisamol T A, Abdulla P
Division of Electronics
Cochin University of Science and Technology
Kochi, India
nisamolshiyas2018@cusat.ac.in

Rekha T K
Department of Electronics
NSS College Rajakumari
Kochi, India
rekhamuralitk@gmail.com

***Abstract*—The novel modified inverted microstrip integrated lowpass-bandpass circuit is developed, fabricated, and experimentally verified. The most of the communication applications prefer to use a lowpass filter prior to a bandpass filter with input and output ports on the same side of the board. The narrow frequency within the C band having a center frequency of 4.7 GHz is passed with a lowpass cut-off frequency of 2.14 GHz. A highly suppressed lowpass stopband of 20 dB up to 13.6 GHz is achieved using an inverted microstrip model with a high Q factor. The bandpass frequency band ranges from 4.6 GHz to 4.9 GHz at the stopband of the lowpass filter and fractional bandwidth of 6.3% is obtained with 27.2 dB passband return loss. The ultra-compact model with a normalized circuit size of 0.0142 λ_g^2 is accomplished.**

Keywords— C band, fractional bandwidth, modified inverted microstrip integrated lowpass-bandpass circuit, Q factor.

I. INTRODUCTION

The lowpass filter circuits are mainly low frequency selective circuits beyond the cut-off frequency associated with certain specific applications. The design considerations should be optimized to provide a sharp roll-off, a wide stopband, and low losses such as return loss, which rely on matching, and insertion loss, which is based on material loss tangent. Triangle-shaped resonators are used to create a microstrip low pass filter with a flat group delay [1]. For wide stopband rejection, several suppressing cells are required, which increases the complexity of the system and results in a substantial return loss. Recently, a planar low pass filter with a meandering uneven 'T' shaped resonator was developed for producing super broad stopbands up to 30 GHz [2] while maintaining attenuation levels of more than 20 dB. Other lowpass resonator structures with better roll-off characteristics are available [3-6]. The level of attenuation of the spurious interferences, on the other hand, is not regulated. There are other lowpass models depicted in [7-8] that have the poor rejection of higher harmonics. Simple high impedance stubs, on the other hand, are highly useful in the receiver areas for constructing lowpass filters with high-frequency rejection and integrating such structures with circuits such as detectors [9]. The bandpass filters have certain frequencies to propagate which depends on the applications. Single bandpass filters are commonly constructed by cascading lowpass and high pass filters, which provide excellent stopband rejection [10]. These structures, however, have a substantial passband return loss. This can be handled by adopting hybrid microstrip/slot line architectures [11], where the lowpass filters are embedded to achieve an ultra-wide out-band. However, as it requires a metallic cage, it will be too bulky for practical uses. Other micro BPF implementation strategies, such as low-temperature semiconductor-based structures [12], mixing lumped and distributed circuits [13], on-chip technology employing meander line resonators [14], and so on, are effective. These bandpass filter circuits suffer several out-band noises since they are embedded in the same circuit board. These interferences between the bands cause reception errors and, in certain cases, information loss. So to avoid such issues and keep the circuit size compact, it is desirable to use integrated technology very effectively. Band selection for multiband [15] receiver applications is demonstrated by the microwave switching mechanism used in [16] with several modes of the integrated lowpass-bandpass system. Using a lumped element switching network without sufficient monitoring, however, there is an inescapable risk of switching error. Furthermore, the response has poor stopband extension because high-frequency interferences occur outside of this range. These structures are used in diplexers [17] and triplexers [18], which have a larger number of ports and lowpass-bandpass resonators. Furthermore, when the number of components in the network grows, the circuit size increase as well, and these integrated architectures have narrower fractional bandwidth for the in-band range.

In the upper microwave and lower millimeter-wave bands, suspended and inverted microstrip lines are among the most possible transmission media. Suspended substrate lines can be used to make the majority of microstrip components, such as power dividers, transistor amplifiers, directional couplers, receiver mixers, and frequency multipliers. The suspended substrate line is particularly beneficial for integrated circuits with waveguide components because of the symmetrical shielding, and the large range of impedance values available makes these media particularly ideal for filters. This work proposes a novel modified inverted microstrip model for the integrated lowpass-bandpass filter circuit. The structure is highly compact with a high Q factor and a higher passband return loss of 27.2 dB is accomplished within the stopband of the lowpass filter. The narrowband having fractional bandwidth of 6.3 % is obtained. The equivalent circuit of each component are separately analyzed and the coupling environment at the elliptic function resonator is compensated by the coupling capacitance. The bandpass response is responsible for this coupling factor and is supported by the cascaded suppressing components.

II. CENTRAL ELLIPTIC FUNCTION RESONATOR (CEFR)

The central elliptic function resonator (CEFR) as shown in Fig. 1(a) is placed on the high impedance transmission line and

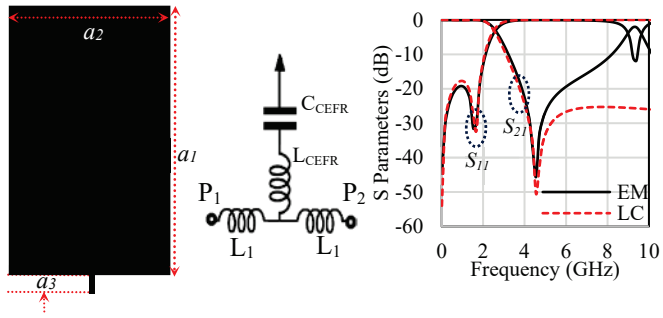

Fig. 1 (a) CEFR model with a_1 = 12.5 mm, a_2 = 4.1 mm and a_3 = 0.7 mm (b) developed equivalent circuit L_1 = 3.65 nH, L_{CEFR} = 0.73 nH and C_{CEFR} = 1.643 pF. (c) The EM and LC simulation comparison.

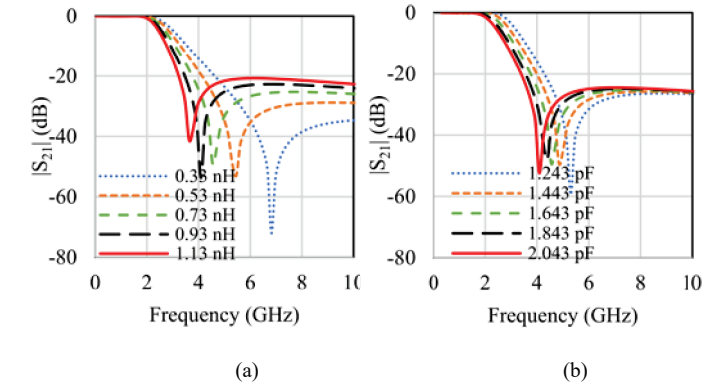

(a) (b)

Fig. 2 The parametric optimization (a) High impedance stub. (b) Low impedance patch.

attained an oscillating electromagnetic field at 4.55 GHz with 50 dB attenuation. The inductors correspond to the high impedance stub and capacitance to the low impedance patch in the elliptic function model. The series combination of these lumped elements analogous to CEFR is shown in Fig. 1(b). The electromagnetic patch resonator and the lumped element model are simulated and compared in Fig. 1(c). The values of the lumped element model depend on the dimensions of the stub and patch, cut-off frequency, characteristic impedances, and the substrate material. The occurrence of transmission zero created by the resonator plays a major role in the stopband frequency characteristics. So, the lumped element values are parametrically optimized to tune the attenuation pole occurrence. The large tuning range of 3.78 GHz to 6.8 GHz is achieved using the inductor values ranging from 0.33 nH to 1.13 nH as illustrated in Fig. 2(a). Alternatively, the lower tuning range is attained with the capacitance value. However, the cut-off frequency can be tuned depending upon the applications. The performance of the CEFR filter is enhanced using suppressing components.

III. SUPPRESSING COMPONENTS

The suppressing components, SC_1 and SC_2, which are a series of high impedance stubs and low impedance patches, are employed here. The suppressing cells are resonators that augment the stopband extension and attenuation level by functioning on the filter structure. This enhancement is due to the high-frequency resonance of these components. The SC_1 and SC_2 have a low impedance patch that is uneven, and this irregularity is exploited in the filter to improve performance. Fig. 3(a) shows the SC_1 structure with the corresponding equivalent circuit loaded on the high impedance stub is given in Fig. 3(b). The resonance of the SC_1 occurs at 9.71 GHz with 55 dB suppression. The SC_2 is having a patch along with a bent high impedance stub as illustrated in Fig. 4(a). The bend compensated capacitance is also associated with the equivalent circuit shown in Fig. 4(b). The SC_2 is having an oscillating electromagnetic field at 7.31 GHz. The EM and LC structures are simulated for SC_1 and SC_2 and given in Fig. 3(c) and Fig. 4(c).

In this work, the transmission line is folded to form a hairpin model which provides coupled line sections. The hairpin transmission line (HTL) increases the coupling impedance which in turn increases the suppression level. The central elliptic function resonator and the suppressing components are loaded on the hairpin transmission line. The use of HTL for the filter circuit has the advantage of providing an ultra-compact unit within the circuit board. The physical size of 11.4 mm x 13 mm is achieved for the circuit.

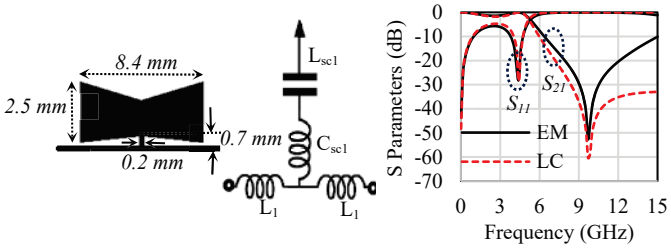

(a) (b) (c)

Fig. 3 (a) The Suppressing component -1 (b) Equivalent circuit with L_{sc1} = 0.59 nH and C_{sc1} = 0.45 pF.

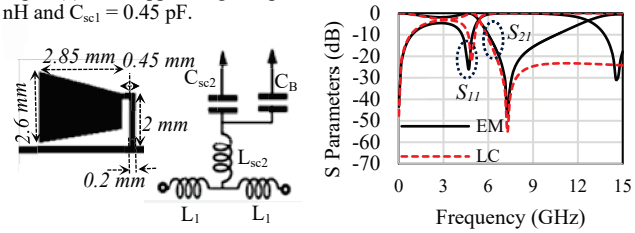

(a) (b) (c)

Fig. 4 (a) The Suppressing component -2 (b) Equivalent circuit with L_{sc2} = 1.8 nH, C_B = 0.07 pF and C_{sc2} = 0.264 pF.

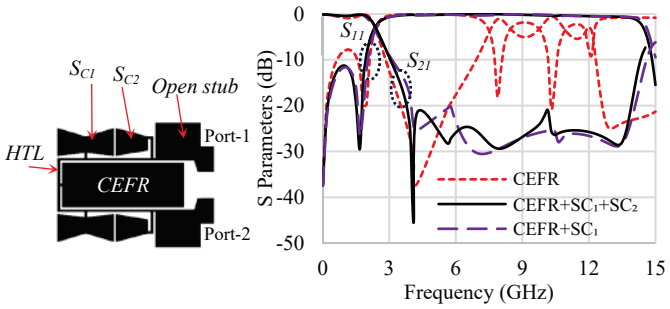

(a) (b)

Fig.5 The simulated cascaded effects of EFR and suppressing components with open stubs. (a) Cascaded structure. (b) Simulation comparison.

The cascaded combination of suppressing components to the central elliptic function resonator improves the impedance characteristics of the overall filter. The lowest impedance provided by the parallel connection of the series inductor and capacitor or associated stub and patch provides an easy path for the signals higher than the cut-off frequency. The effect of the cascaded combination along with the open stubs is shown in Fig. 5(b).

IV. MODIFIED CEFR FOR INTEGRATED RESPONSE

The single layer (SL) central elliptic function resonator is modified to obtain a bandpass response in between the stopband of the lowpass response. The coupling between the patch section and the open stub has increased by modifying the dimensions with irregular shapes. The coupling environment created by this modification provides a narrow passband around 4.7 GHz with 51 dB suppression. The angular cut of θ^0 given to the end of the patch is optimized and the return loss is significantly improved at 75^0. The in-line nature of input and output ports strengthens the narrowband coupling and reduces radiation loss.

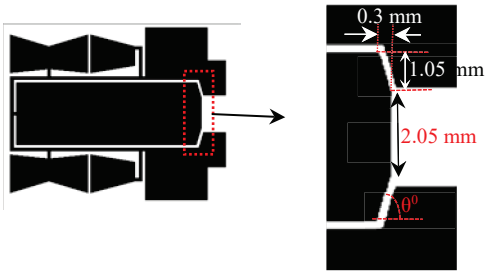

Fig 6 The planar structure of modified CEFR (SL model) and the dimensions.

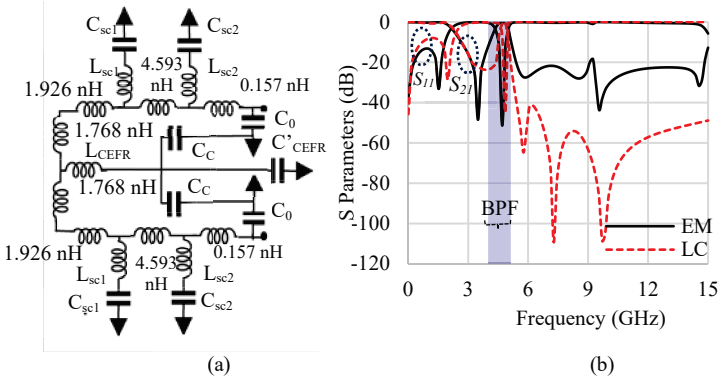

Fig. 7 (a) Developed equivalent circuit. (b) EM and LC comparison results.

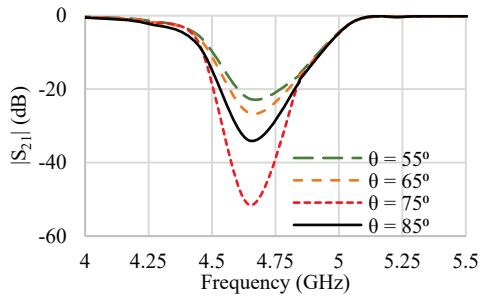

Fig. 8 (a) Parametric analysis of the angular cut angle of the modified CEFR.

V. MODIFIED INVERTED MICROSTRIP INTEGRATED FILTER

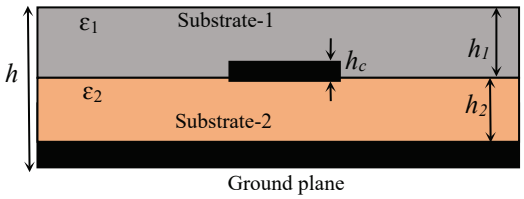

Fig. 9 Modified inverted microstrip model (MIM model)

In order to improve filter performance, there are numerous derivates of microstrip lines. Suspended/inverted microstrip lines are used in the filter implementations. Inverted lines are having a high Q factor which enhances the attenuation behaviour of the filter. The air in the inverted model is replaced by a dielectric substrate with dielectric constant ε_1 as illustrated in Fig. 9. Table I gives the values of parameters of the MIM model.

TABLE I. DIMENSIONS OF MIM MODEL

Dimensions	ε_1	ε_2	h_1	h_2	h_c
Values	4.4	2.2	0.8 mm	0.79 mm	0.034 mm

The prototype with a separate top and bottom layer is shown in Fig. 10(a-b). The filter structure provides fractional bandwidth of 6.3% with a central frequency of 4.7 GHz. The return loss enhancement of 62 dB is achieved using the inverted microstrip technique.

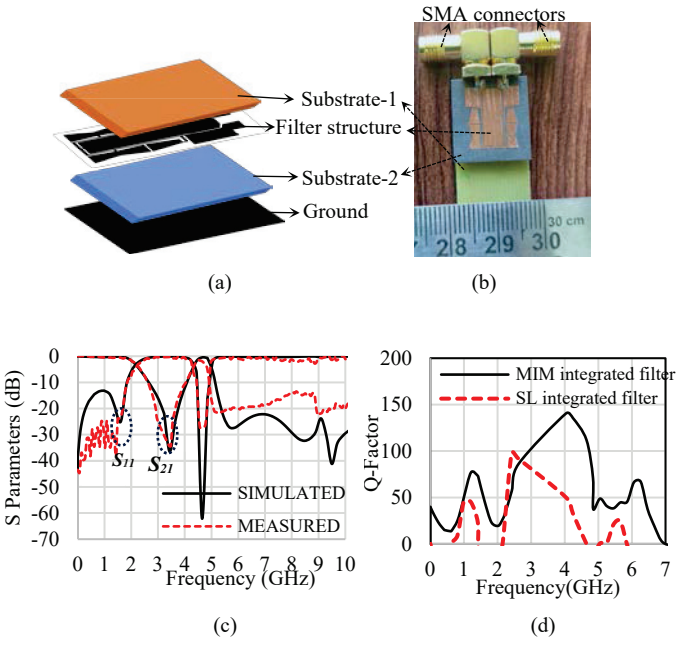

Fig. 10 (a)The modified inverted model (b) Fabricated prototype (Before fixing top layer). (c) Measurement results compared with simulation (d) Q factor improvement of MIM integrated filter.

Fig. 10(c) shows the measured and simulated frequency characteristics with a proper MIM integrated filter. Photo etching is used to create the structure, and the Rohde and Schwarz ZVL vector network analyzer is used to measure it at up to 13.6 GHz. The results using MIM model illustrates the improved attenuation characteristics at the passband of the bandpass response compared to the single-layer integrated filter. The improvement in the Q factor while using the MIM model compared to the SL model of the integrated circuit is illustrated in Fig. 10(d). As the circuit is of high Q factor, the narrow bandwidth is accomplished. Table II displays the performance comparison of the proposed integrated filter with other related works of literature.

TABLE II. COMPARISON OF INTEGRTED MIM FILTER WITH OTHER LITERATURES

Reference	**Response**	f_c **(GHz)**	**FBW (%)**	**Passband Return-loss**	**Physical Size (mm^2)**
[11]	BPF-LPF	1.9	12.63	23	15.5 x 7.2
[12]	BPF-LPF	2.4	9	10	NM
[13]	BPF-LPF	2.4	7.6	NM	NM
[14]	BPF-LPF	2.4	10	14.5	70 x 42
[15]	BPF-LPF	6.34	24	20.6	16.9 x 11.7
This work	BPF-LPF	4.7	6.3	27.2	11.4 x 13

VI. CONCLUSION

Using an inverted microstrip model, a novel integrated lowpass-bandpass circuit is created and experimentally validated. Most communication applications prefer a bandpass filter with input and output ports on the same side of the board over a lowpass filter. A lowpass cut-off frequency of 2.14 GHz is used to pass through the C band portion. The use of a modified inverted microstrip model with a high Q factor results in a highly suppressed response. With 20 dB rejection of high-frequency spurious noises from other circuits, the bandpass central frequency of 4.7 GHz is produced at the stopband of the lowpass filter. It is possible to utilize the proposed ultra-compact MIM model for the C band communication applications.

REFERENCES

[1] K. Ali, F. Shama,"Compact Microstrip Low Pass Filter with Flat GroupDelay using Triangle shaped Resonators", Int. J. Electron. Commun. (Aeü), Vol. 83, pp. 433–438, 2018

[2] F.Shama, M. Hayati, M. Ekhterae, "Compact Microstrip Lowpass Filter using Meandered Unequal T-Shaped Resonator with Ultra-Wide Rejection Band", Int. J. Electron. Commun. (Aeü), vol. 85, pp. 78–83I, 2018.

[3] Karimi, G., Lalbakhsh, A. and Siahkamari, H., Design of sharp roll-off lowpass filter with ultra wide stopband. IEEE Microwave and Wireless Components Letters, Vol. 23, No. 6, pp. 303-305, 2013.

[4] Xiao, M., Sun, G. and Li, X., A lowpass filter with compact size and sharp roll-off. IEEE Microwave and Wireless Components Letters, Vol. 25, No. 12, pp. 790-792, 2015.

[5] Mousavi, S.M.H., Makki, S.V.A.D., Siahkamari, H., Alirezaee, S. and Ahmadi, M., Performance improvement of microstrip LPF based on transfer function analysis. IEEE Microwave and Wireless Components Letters, Vol. 26, No. 5, pp. 322-324, 2016.

[6] Nisamol, T.A., Abdulla, P. and Raphika, P.M., Dual split resonator lowpass filter with ultra-wide stopband and sharp roll-off rate. IET Microwaves, Antennas & Propagation, Vol. 14, No. 12, pp. 1462-1468, 2020.

[7] Li, L., Li, Z.F. and Mao, J.F., Compact lowpass filters with sharp and expanded stopband using stepped impedance hairpin units. IEEE Microwave and Wireless components letters, Vol. 20, No. 6, pp. 310-312, 2010.

[8] Velidi, V.K. and Sanyal, S., Sharp roll-off lowpass filter with wide stopband using stub-loaded coupled-line hairpin unit. IEEE Microwave and Wireless Components Letters, Vol. 21, No. 6, pp. 301-303, 2011.

[9] Moloudian, G., Bahrami, S. and Hashmi, R.M., A microstrip lowpass filter with wide tuning range and sharp roll-off response. IEEE Transactions on Circuits and Systems II: Express Briefs, Vol. 67, No. 12, pp. 2953-2957, 2020.

[10] Chen, N.W. and Fang, K.Z., An ultra-broadband coplanar-waveguide bandpass filter with sharp skirt selectivity. IEEE microwave and wireless components letters, Vol. 17, No. 2, pp. 124-126, 2007.

[11] Li, R. and Zhu, L., Ultra-wideband (UWB) bandpass filters with hybrid microstrip/slotline structures. IEEE microwave and wireless components letters, Vol. 17, No. 11, pp. 778-780, 2007.

[12] Setoodeh, S., Laforge, P.D. and Mansour, R.R., Realization of a highly miniaturized wideband bandpass filter at the UHF band. IEEE transactions on applied superconductivity, Vol. 21, No. 3, pp. 538-541, 2010.

[13] Zhang, R. and Peroulis, D., 2018. Mixed lumped and distributed circuits in wideband bandpass filter application for spurious-response suppression. IEEE Microwave and Wireless Components Letters, Vol. 28, No. 11, pp. 978-980, 2018.

[14] Xu, K.D., Zhu, X., Yang, Y. and Chen, Q., A Broadband On-Chip Bandpass Filter Using Shunt Dual-Layer Meander-Line Resonators. IEEE Electron Device Letters, Vol. 41, No. 11, pp. 1617-1620, 2020.

[15] Choudhary, D.K. and Chaudhary, R.K., Compact lowpass and dual-band bandpass filter with controllable transmission zero/center frequencies/passband bandwidth. IEEE Transactions on Circuits and Systems II: Express Briefs, Vol. 67, No. 6, pp. 1044-1048, 2019.

[16] Deng, P.H., Tsai, J.T. and Liu, R.C., Design of a switchable microstrip dual-band lowpass-bandpass filter. IEEE Microwave and Wireless Components Letters, Vol. 24, No. 9, pp. 599-601, 2014.

[17] Deng, P.H. and Tsai, J.T., Design of microstrip lowpass-bandpass diplexer. IEEE microwave and wireless components letters, Vol. 23, No. 7, pp. 332-334, 2013.

[18] Chen, F.C., Qiu, J.M., Hu, H.T., Chu, Q.X. and Lancaster, M.J., Design of microstrip lowpass-bandpass triplexer with high isolation. IEEE Microwave and Wireless Components Letters, Vol. 25, No. 12, pp. 805-807, 2015.

[19] Nisamol, T.A., Abdulla, P. and Rekha, T.K., "Integrated Lowpass and C Spectrum Band Pass Filter using Miniaturized Stub Based Model", AEU-International Journal of Electronics and Communications, p.154080, 2022.

[20] Rekha, T.K., Abdulla, P., Raphika, P.M. and Jasmine, P.M., Compact microstrip lowpass filter with ultra-wide stopband using patch resonators and open stubs. Progress In Electromagnetics Research, Vol. 72, pp. 15-28, 2017